報 文
화학공학 제12권, 제1호
J. KIChE, Vol. 12 No 1
Feb. 1974

酸化鐵還元에 대한 添加物의 効果

柳 慶 玉
漢陽大學校 工科大學 化學工學科

(접수 1974. 1. 17)

Effect of Additives on the Reduction of Hematite

Kyong Ok Yoo

Dept. of Chem. Eng., College of Eng, Hanyang Univ., Seoul, Korea

요 약

수소로 산화철을 환원시킬 때 환원속도에 미치는 첨가물의 효과와 역활을 규명하기 위하여 산화철의 중량감소, 격자정수, 전기전도도를 측정하였다. 그 결과 Li_2O는 환원속도와 전기전도도를 증가시켰고 Al_2O_3와 Ga_2O_3는 감소시켰는데, α-Fe_2O_3의 결손구조와 전자이동기구로서 이를 설명하였다.

한편 280°~425°C의 실험범위에서 α-Fe_2O_3는 금속철로 직접 환원되었으며, 모든 속도론적 Data는 Avrami식에 잘 맞았다.

Abstract

To clarify the effect of additives on the reduction rate of hematite with hydrogen and the role of additives, the loss of weight, the lattice constant, and the electrical coniductvity have been measured for pure and doped hematite. The reduction rate was increased and the electrical conductivity was decreased by the addition of Li_2O and trivalent oxi]es (Al_2O_3 and Ga_2O_3) The effect of additives on the electrical conductivites is discussed in term of electron transfer mechanism. In the temperature range of 280°to 425°C, hematite is directly reduced to metallic iron. The kinetic data show good agreement with Avrami equation.

I. Introduction

The investigation of the reduction of iron oxides with hydrogen has been studied by many investigators. Their study was partly practical, dealing with reduction process, and partly theoretical, involving comprehensive labolatory experiments for the effect of temperature, pressure, gas composition and the shape of iron oxide on the reduction rate. Despite the numerous papers on

the reduction of iron oxide, a few papers concerning the additive or impurity effect on this important metallurgical and industrial processes were reported. Since Schenck and his coworkers[1] suggested that the rate of reduction was accelerated when lime was added to wustite in 1929, some papers were reported on this very interesting process. Williams and Ragatz[2,3] found that potassium and sodium carbonates increased the reduction rate of magnetite ore. Mcgeorge et al.[4] found that the addition of Na_2O_3 to the iron ore such as Cuban lateritic hematite and Cornwall dense magnetite increased the reduction rate and addition of Na_2O to chemical pure grade Fe_2O decreased the reduction rate with hydrogen. From this result they concluded that the additive, alkali oxides, apparently reacted with the impurities in ores freeing the iron oxide for reduction. Morawietz et al.[5] recognized additional effect of iron powder and other metals such as nickel, cobalt and copper on the reduction of magnetite. Recently Khallafalla and Weston[6] also studied additive effect of alkali and alkaline earth oxide on the reduction of wustite pellet with carbon monoxide at 1000°C and found that small amount of additive (below 0.69 atomic %) had a strong accelerating effect on the reduction rate of wustite to metallic iron. The extent of the reduction rate enhancement was proportional to ionic radius and electronic charge of the additives. On the other hand, Tigershold[7], Edstrom[8] and Esche and Steinhauer[9] reported the accelerating effect of calcium compound additives on the reduction rate of hematite or magnetite.

As mentioned above, although the addition of impurities to iron oxide accelerates the reduction rate, the role of additives on the reduction and the actual mechanism of the reduction process of iron oxides have not been clarified. The aim of the present work is to clarify the role of additives in the reduction of hematite based on the defective structure of hematite.

II. Experimental

Preparation of Sample: Hematite was prepared from chemical pure grade ferrous oxide (99.9%). Ferrous oxide was oxided for 4 hrs at 700°C in air and quenched to room temperature in air. X-ray diffraction data of the resulting materials showed the same pattern as α-Fe_2O_3. Lithium, aluminium and gallium nitrate were used as the additives. These additives were selected as their ionic radius are nearly equal to that of iron ion. Their ionic radius and other properties were shown in Table 1 and compared with that of hematite (α-Fe_2O_3).

Doping was made as follows: (1) Aknown weight of an additive was dissolved in distilled water, (2) a known weight of hematite was mixed with above additive solution, (3) the solution was completly dried with infrared lamp while being agitated continueously for about 1 hr, and the resulting agglomerate was pulverized, (4) the doped hematite was slowly heated from room temperature to the melting point of the additive and for 1 hr at temperature which is 20°C heigher than melting point of the additive, and finally heated for 6 hrs at 1000°C in air followed by quenching to room temperature in air, (5) the resulting oxide was pulverized and then kept in a desicator. Hematite sample was also heated for 6 hrs at 1000°C in air to make the same condition with all doping samples.

X-ray Analysis: Hematite and all doped samples were analyzed by the X-ray diffractometer (Holland Phillps PW-1051) for measuring the lattice constant and for the identification. X-ray operating conditions were: Target CoKα; filler Fe: voltage 30kV; current 10mA; counter G.C.; full scale counts 800 cps; scanning speed $2°2\theta$/min and angle range 20~80°. In the measurements of lattice constants, scanning speed was one-fourth degree in 2θ per minute, time constant 4 sec and angle range from 150_o to 50°. The reduction products were also analyzed.

Electrical Conductivity: Conductivities of all 0.5 atomic% doped sample and pure hematite were measured.[10] The pellets with 10mm in diameter and about 5mm in length were used as samples of electrical conductivity.

Other Measurements: Surface area of all samples were measured by the B.E.T. method. The sizes of particle of all samples were measured and the shape of the samples and some reaction products were observed

with a electron microscope.

Apparatus and Method: The experimental apparatus as shown in Fig. 1 consists of four main parts: the gas flow control system, a vacuum line, the microbalance system, and the temperature control system. The hydrogen gas from the stock bomb is introduced to the top of reaction tube through the vacuum line and flow down around the platinum sample basket and flow out at the bottom. The size of the platinum sample basket is 15mm in diameter and 4mm in length. The flow rate of hydrogen was controlled by a reducing valve and measured with a calibrated venturi flow meter. Water in hydrogen was frozen out in a liquid nitrogen trap attached to the vacuum line. The gas left the system through the liquid paraffin trap which was attached to prevent the back flow of air. An electrical resistance furnace which is movable in vertical directions was fitted around the reaction tube. Temperature was automatically controlled by a Pt and Pt-13%Rd thermocouple located near the furnace wall and measured by the same type of thermocouple located just upper the sample basket.

The hydrogen gas was introduced into the reaction tube evacuated to 10^{-3} torr at the desired temperature. An ionization gauge and a Pirani gauge used for measuring the pressure. A loss-in-weight was measured by the Shimadzu Recording Micro-Balance (Type RMB 50V) and automatically recorded by the TOA Electronic Polyrecorder (model EPR 10A).

The experiments were carried out as follows: (1) a platinum sample basket containing the sample of 40 mg was suspended by a fine platinum wire attached to the top of the microbalance beam, (2) air in the quartz reaction tube was evacuated by a vacuum pump to about 10^{-3} torr, (3) the quartz reaction tube was heated to the experimental temperature, (4) the hydrogen gas was introduced into the reaction tube and from that time the loss-in-weight was meaured. When the reduction was finished, hydrogen gas in the reaction tube was evacuated to 10^{-3}torr, quenched to room temperature, filled with high purity nitrogen to 1 atmosphere, and then stand for about 24 hrs. The products were used for X-ray analysis and electromicroscopic observation.

The range of experimental temperature were from 280° to 425°C. The influence of hydrogen flow rate on the reduction rate was checked at 300°C. As shown in Fig. 2 there is no influence of the flow rate of hydrogen on the reduction rate beyond the flow rate of 57 cc/min. Therefore, this experiment was performed

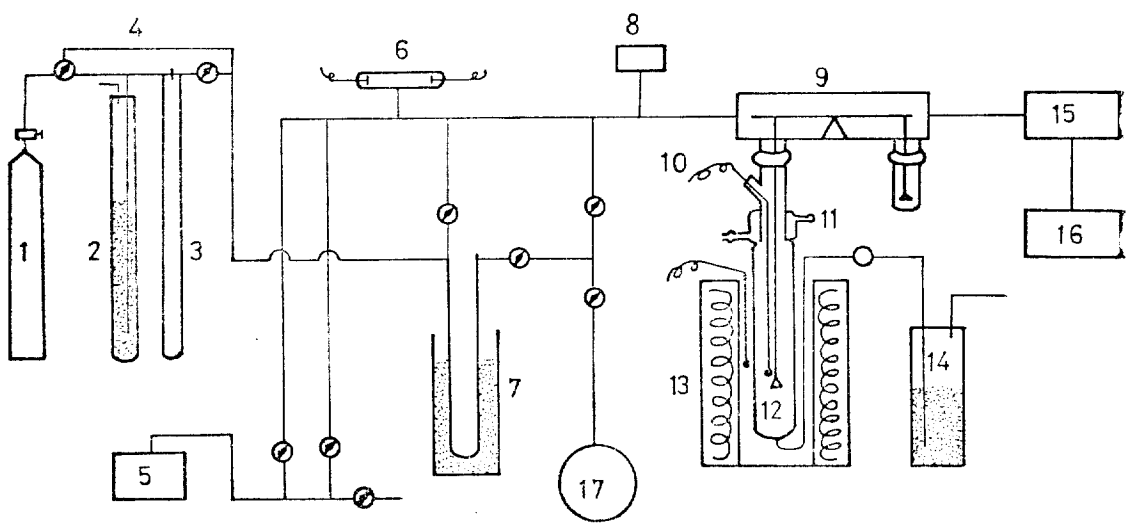

1. hydrogen bomb 2. water cylinder for flow rate control 3. venturi manometer 4. by-pass line 5. rotary pump
6. ionized gauge 7. liquid nitrigen trap 8. Pirani gauge 9. micro-balance(Shimadzu RMB-50V) 10. Pt-Pt-13%Rd thermocouple
11. water condenser 12. platinum sample basket 13. electrical furnace 14. liquid paraffin trap 15. controller of balance (Shimadzu RMB-50V) 16. electronic polyrecorder (TOA EPR-10A) 17. N_2 gas

Fig. 1 Schematic Diagram of Experimental Apparatus

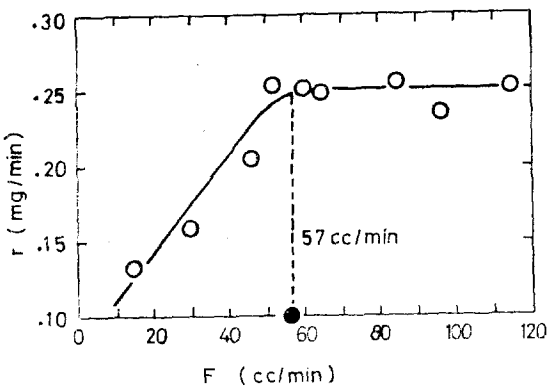

Fig. 2 Infuence of the Flow rate of Hydrogen on the Reduction Rate of Pure Hematite at 300°C

at constant flow rate of 57 cc/min which corresponds to a linear gas velocity of 0.1 cm/sec in the reaction tube.

III. Results

The physical properties of the pure and doped hematite are given in Table 1. The particle size distribution of the pure and doped hematite ranges from 0.47 to about 4μ and from 0.94 to 3.14μ, respectively. Surface area was 0.74m²/gr for pure hematite and 1~0.5m²/gr for all doped samples. The surface area of 0.7~1.0 m²/gr for doped and pure hematite was very small in comparison with 10m²/gr for the natural hematite. Lattice constant in Å unit as a function of additive contents is shown for three doped samples in 280° to Fig. 3. The lattice constant obvioiously decreases with increasing contents of additive except for that of pure hematite. With this exception, the trend of curves agrees with Vegard rule[16] stating that the lattice parameter of solid solution linearly increases or decreases with the content of a consistituent component. For the system of Fe_2O_3-Li_2O, α-lithium ferrite ($LiFe_5O_8$) was found from the X-ray diffraction data. For Al_2O_3 and $G\alpha_2O_3$ doped samples, no compound formation was obserbed.[18]

The fraction of reaction(α)-time curves are sigmoiddal having the induction time of relatively long duration. The time decreased with the increasing temperature and the addition of time. The induction time (t_0) and corrected 50% reduction time are shown in Table2. The corrected 50% reduction time ($t_{0.5R}$) was defined as follows; $t_{0.5R}=t_{0.5}-t_0$ where $t_{0.5}$ is the time which is necessary for the 50% reduction. The result for Li_2O doped sample is given in Fig. 4. The effects of the reaction and 50% reduction time at above 340°C were small and those under 340°C were very large. are shown in Fig. 5 for pure and 0.5% doped samples. Fig. 6 show the effect of additive contents at 380°C. All of the reduction data in the temperature range of 425°C are expressed with Avrami equation [11] [12] that was derived under the assumption of the phase boundary controlled reaction. The results are shown in from Fig. 7 to Fig. 9 and the rate constant calculated

Table. 1 The Physical Properties of the Pure and Doped Hematite, and the Additives

Additive / Additive Content(at. %) / Properties	Li_2O			Al_2O_3			Ga_2O_3			Hematite α-Fe_2O_3
	0.5	1.0	2.0	0.5	1.0	2.0	0.5	1.0	2.0	
Particle Size (μ)	0.47 −3.93	0.47 −4.40	0.47 −4.04	0.47 −4.40	0.47 −4.04	0.47 −4.04	0.47 −3.39	0.47 −3.14	0.47 −4.40	0.94~3.14
Surface Area (m²/gr)	0.91	0.70	0.44	0.97	0.99	0.77	0.99	0.75	1.17	0.74
Lattice Constant (Å)	5.4251	5.4230	5.4228	5.4176	5.4239	5.4204	5.4239	5.4237	5.4240	5.4228
Activation Energy (kcal/mole)	15.15	16.18	16.43	19.65	19.27	18.90	19.03	20.56	21.67	16.08
Solid Solution	$LiFe_5O_8$			none			none			
Ionic Radius (Å)	Li^{1+} 0.61			Al^{3+} 0.57			Ga^{3+} 0.62			Fe^{3+} 0.67
System	Cubic			Trigonal			Rhombohedral			Rhombohedral
Original Form	$LiNO_3$			$Al(NO_3)_3$ $9H_2O$			$Ga(NO_3)_3$ $8H_2O$			
Melting Point (°C)	261			73			110			1560
Molecular Weight	68.95			375.15			399.87			159.70

Table 2. Induction Time (to) and Corrected 50% Reduction Time ($t_{0.5}R$) in Minutes

Temp°C \ Additives / Additive Contents (atomic %)		Li_2O			Al_2O_3			Ga_2O_3			α-Fe_2O_3
		0.5	1.0	2.0	0.5	1.0	2.0	0.5	1.0	2.0	
280	t_0	24	28	30	90	70	50				20
	$t_{0.5R}$	174	93	92	190	167	160				52
300	t_0	8.5	14.5	17.0	10.0	36.0	32.0	40.0	80.0	110.0	15
	$t_{0.5R}$	36.5	41.5	58.0	113.0	94.0	93.0	114.0	160.0	?	51.0
320	t_0							30.0	50.0	60.0	12.0
	$t_{0.5R}$							62.0	83.0	152.0	43.0
340	t_0	6.6	7.7	8.0	15.0	10.0	4.0	8.3	15.0	20.0	8.0
	$t_{0.5R}$	17.1	23.3	27.3	37.0	39.0	34.0	44.7	44.0	62.0	24.0
380	t_0	0.0	0.0	0.0	3.3	0.5	0.5	5.0	7.0	10.0	2.5
	$t_{0.5R}$	8.0	8.3	9.3	10.5	13.5	10.5	22.0	20.0	25.0	8.5
400	t_0	0.0	0.0	0.0	2.0	0.3	0.0	1.0	1.0	3.0	1.6
	$t_{0.5R}$	6.0	5.3	6.3	14.0	9.7	6.0	11.0		20.0	7.9
425	t_0	0.0	0.0	0.0	1.0	0.0	0.0	0.0	0.0	3.0	0.0
	$t_{0.5R}$	3.8	0.0	4.3	11.0	6.0	3.0	4.0	6.0	15.0	4.0

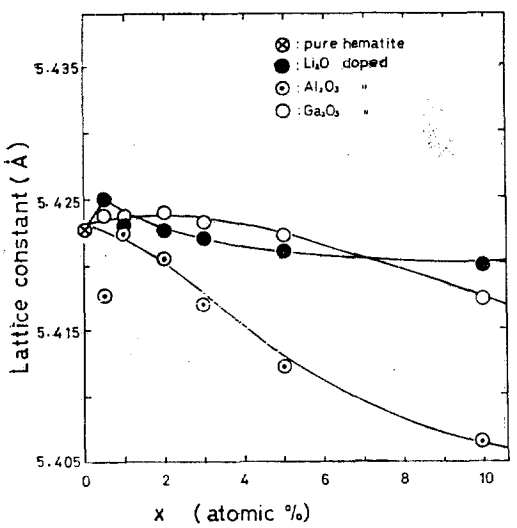

Fig. 3 Change of Latlice Constant of Sample with Dopant Contents

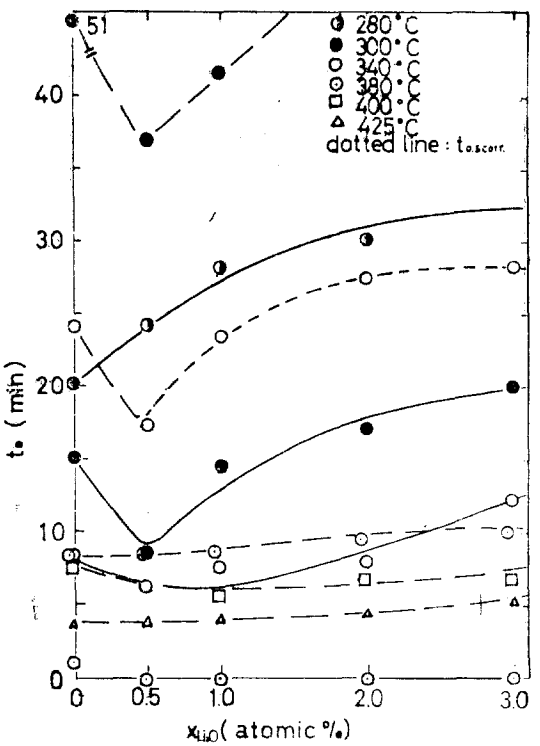

Fig. 4 Relation between Dopant Content on Induction Time (on corrected 50% Reduction) Time at Various Temperature

from Avrami plot are plotted against 1/T in Fig. 10, 11 and 13.

Table 1 shows the activation energies for each samples (in the temperature range of 280° to 425°C) calculated from Arrhenius plot. The energies of activation for pure hematite are 16.1 kcal/mole. This value is the same with 15.3 kcal/mole by Mcgeorge,[4] 16.57 kcal/mole by Feinman[13] and 15.45 kcal/mole Mckewan[14] measured at the same temperature ranges In these figures, the reductivity of samples obviously decreases with increasing the dopant contents except Al_2O_3 doped sample. For Al_2O_3 doped sample, the reductivity decreasesby doping, however, the quantitative effect of the additive contents was not obuious. The rate constants obtained at 300°C and 400°C are

plotted a function of the additive contents in Fig. 13. The rate constants of Li_2O and Ga_2O_3 doped samples decrease with increasing the additive contents and in the case of Al_2O_3 increases with additive content up to 2.0 atomic%. All the results obtained

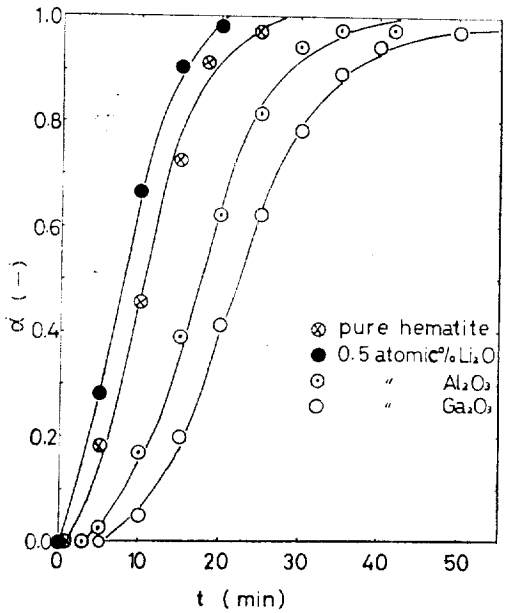

Fig. 5 Effect of Dopants on the Redution of Hematite at 380°C

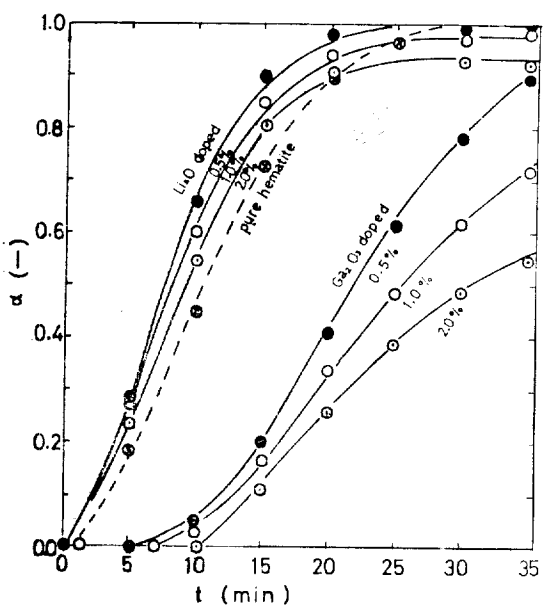

Fig. 6 Effects of Dopants and Their Content on the Reduction of Hematite at 380°C

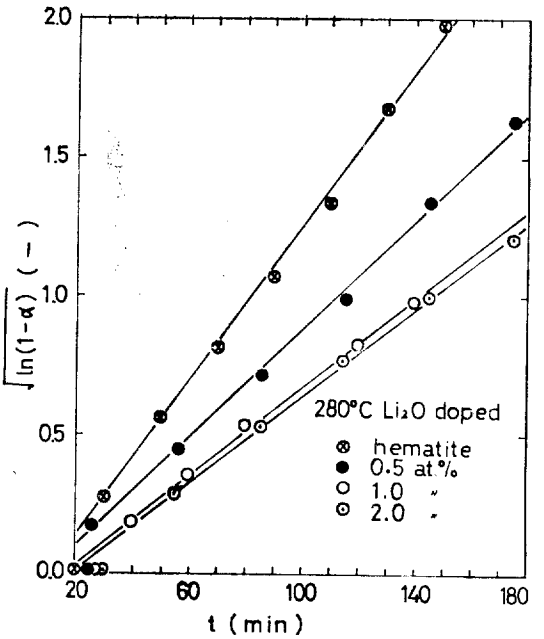

Fig. 7 Avrami Plot for Li_2O Doped Hematite at 280°C

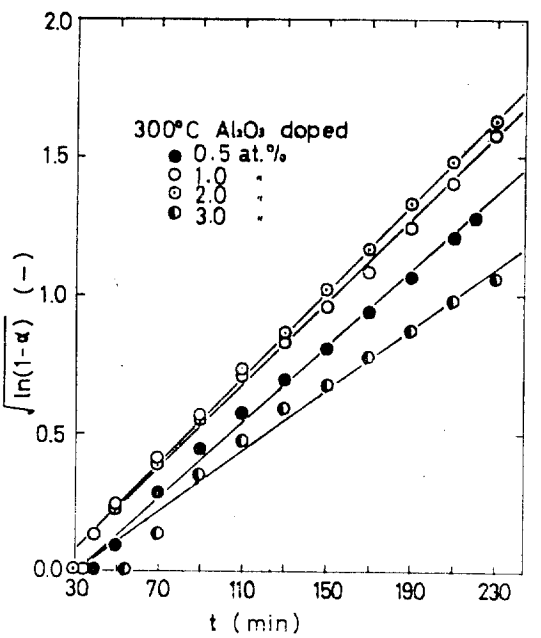

Fig. 8 Avrami Plot for Al_2O_3 Doped Hematite at 300°C

for three additives can not be shown in Fig. 14, however, the trend is the same in all temperature range.

For the understanding of the reduction processes, the

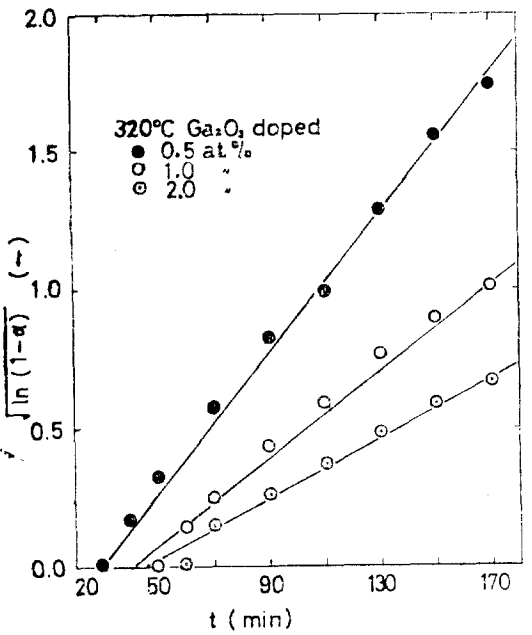

Fig. 9 Avrami Plot for Ga_2O_3 Doped Hematite at 320°C

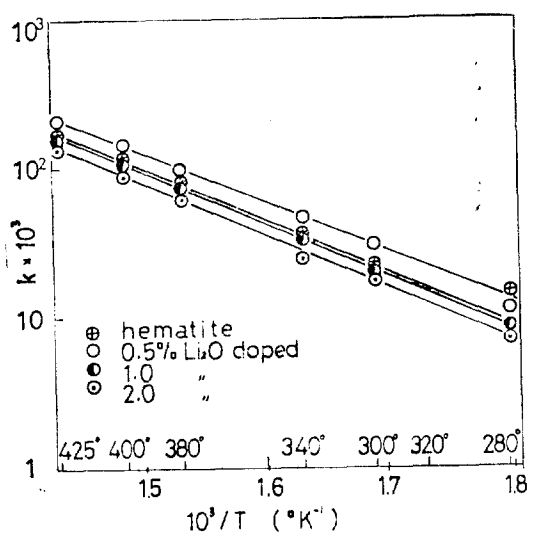

Fig. 10 Temperature Dependence of Pure and Li_2O Doped Hematite

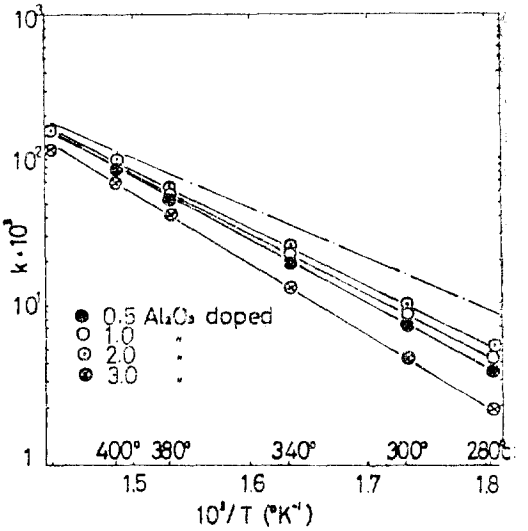

Fig. 11 Temperature Dependence of the Rate Constant of pure and Al_2O_3 Deped Hematite

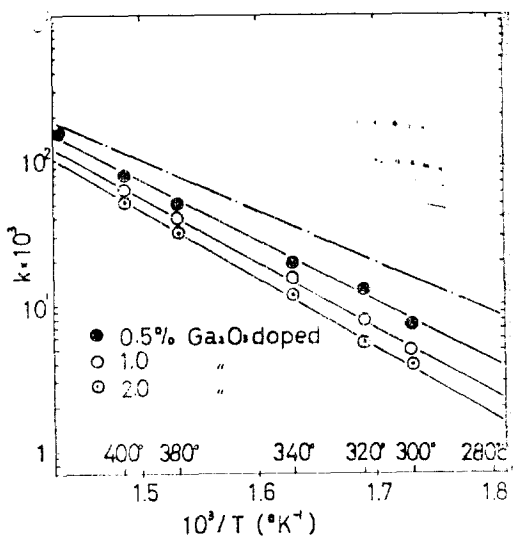

Fig. 12 Temperature DepenPence of the Rate Constant of Pure and Ga_2O_3 Doped Hematite

reduction was stoped by quenching at various stages and after letting it stand for 24 hrs in nitrogen gas. The product was analyzed with X-ray. All the X-ray diffraction data revealed that the product was composed of maehtite and metallic iron. This result represents that the hematite was directly converted to metallic iron without passing through other intermediates such as magnetite, wustite and other complex compounds.

Finally, in order to clarify the structure of doped samples and the role of the dopants in the reduction, the electrical conductivities of 0.5 atomic % doped samles and pure hematite were measured under 2.2×10^{-3} torr and shown as a function of reciprocal temperature in Fig. 14. The electrical conductivity of the

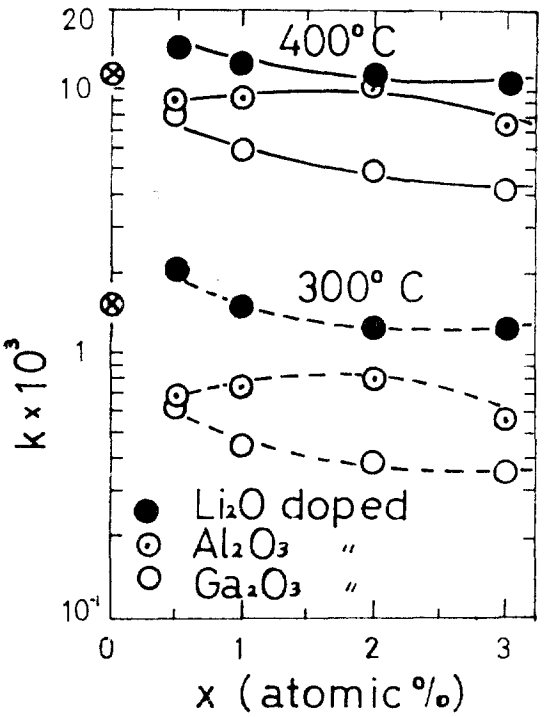

Fig. 13 Effect of Dopant Contents on the Reduction Rate at 300° and 400°C

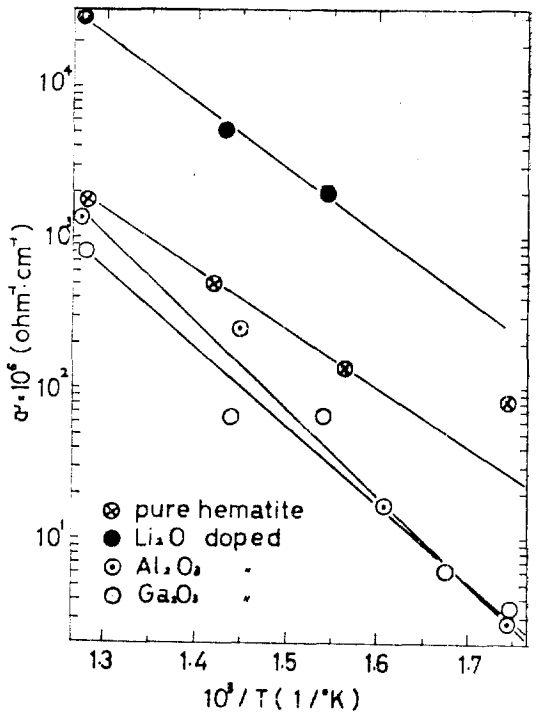

Fig. 14 Temperature Dependence of Electrical Conductivity of Pure and Doped Hematite at 2.2×10^{3} torr in Air.

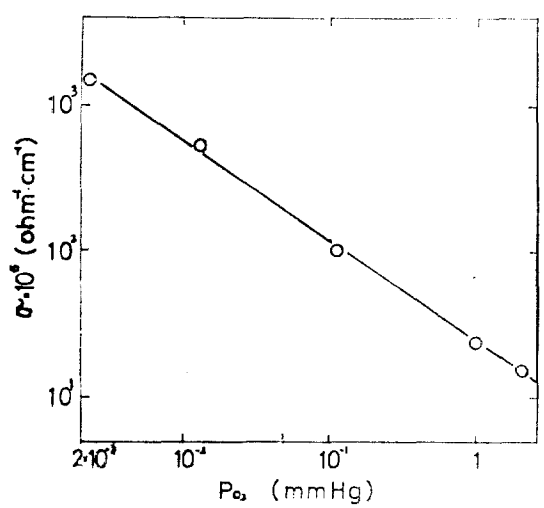

Fig. 15 Electrical Conductivity of Pure Hematite as a Function of Oxygon partial Pressure at 515°C

Li_2O doped sample was approximately tenfold greater than that of pure hematite and those of Al_2O_3 and Ga_2O_3 doped sample were about onef-ifths throughout the temperature ranges studied. Fig. 15 shows the electrical conductivities of pure hematite as a function of oxygen partial pressure at the constant temperature of 515°C. The conductivity decrease quickly at initial stage and slowly at more than 2 hrs. Therefore, the measurement was made at 2 hrs. The electrical conductivity decreases with increasing the oxygen partial pressure. This result suggests that hematite used is a n-type semiconductor.

Discussion

The difference in the reactivity of the samples may be ascribed to the difference in the defective structure of hematise. Hematite (α-Fe_2O_3) is rhombohedral crystal with the lattice constant of a=5. 4228 Å and x=55. 17°. The O^{2-} ions are arranged in a close-packed hexagonal lattice and two-thirds of the octahedral interstices are occupied by Fe^{3+} ions. This oxide has

a small oxygen deficit and iron ions is probably in additional interstitital positions. Tannhauser[15] suggested the existence of interstitial Fe^{2+} ion. Whereas the electrical conductivity plotted against oxygen partial pressure in Fig. 15 suggests that hematite is possibly n-type semiconductor. However, the effect of dopants (Li_2O, Al_2O_3 and Ga_2O_3) in the electrical conductivity suggests that hematite is p-type. No agreement between both results was obtained.

Tanhauser[15] proposed that the mechanism of the conductivity in hematite is the electron transfer between Fe^{3+} and Fe^{2+} ions in the octahedral position. The Fe^{2+} ions in hematite are incorporated by the oxygen deficit and considered to be located at the interstitial positions. However, no definite structure is given.

With these considerations concerning the defective structure of hematite, the authors tentatively assume the defective structure as follows:

$$Fe_2O \rightarrow Fe^{3+}_{2-2X}(oct)\cdot Fe^{2+}(int)\ \ O_{3-X} + XFe^{2+}(int) + \frac{X}{2}O_2(g) \qquad (1)$$

Equation (1) states that each half of Fe^{2+} ions occupies the octahedral and the interstitial positions. The assumption of the equal distribution of Fe^{2+} ions will not change essentially the character of foregoing discussions. From equation (1), the concentration of $[Fe^{2+}(int)]$ is obtained to be proportional to $Po_2^{-1/2}$ and equal to that of $[Fe^{2+}(oct)]$. The conductivity by the electron transfer is proportional to the product $[Fe^{3+}(oct)]\cdot[Fe^{2+}(int)]$ and $[Fe^{3+}(oct)]\rightarrow[Fe^{2+}(oct)]$. Thus, the conductivity is expected to proportional to $[Fe^{2+}(int)]$ and to $Po_2^{-1/2}$. The pressure dependency of the conductivity was proportional to $Po_2^{-1/1.4}$ and the discrepancy between the theoreical and experimental is not so large in view of the rough assumption made previously.

If dopant Li_2O incorporated in hematite substitutes the interstitial Fe^{2+} ion expelling the Fe^{2+} ions to the octahedral position, the probability of the electron transfer will increase and the conductivity is expected to increase. If trivalent metallic ions (Al^{3+} and Ga^{3+}) incorporated occupy the octahedral, the probability of the electron transfer decrease and the low conductivity of Al^{3+} and Ga^{3+} doped samples is reasonable. Further study on the distribution of the doped ions will be done to verify the above discussion.

As for the reactivity of doped hematite, the elucidation of the effect of dopants seems to be more difficult because the detailed defect structure of hematite is not clear. The increase of Fe^{3+} ion in the octahedral position due to the incorporation of Al_2O_3 and Ga_2O_3 seems to result the more stoichiometric composition than pure hematite. The more stoichiometric compound is expected to have the less reducibility. Li_2O doped hematite may be considered to have the more defective than pure hematite and therefore, to have the high reactivity.

The alternative elucidation for Li_2O doped sample have to be discussed here. Roy and et al.[17] have presented the phase diagram of Fe_2O_3–Li_2O system. The phase diagram states that Li_2O makes no solid solution with hematite and only lithium ferrite coexisting with hematite as a mixture. Therefore, lithium ferrite particles are thought to be dispersed homogeneously in hematite. The texture seems to increase the reactivity of doped hematite. The disperesed ferrite may retard the mutual sintering of iron particles and hold a good condition for further progress of the reaction.

Conclusion

1. In the temperature range of 280° to 425°C hematite directly change to metallic iron.
2. The kinetic data for the reduction of pure and doped hematite are successfully expressed by Avrami equation.
3. The reduction rate increases and the electrical conductivity decreases for the Li_2O and trivalent oxides (Al_2O_3 and Ga_2O_3) studied.
4. The effect of dopants on the electrical condu ctivity is discussed with the electron transfer mechanism.

Acknowledgments

This investigation was carried out at the Komatsu Laboratory, Department of Chemical Engineering, Tokyo Institute of Technology, by the fund of

Japanese National Commission For UNESCO. The author thanks all collaborators at Komatsu Laboratory and UNESCO office for valuable help with investigations. For advice on the X-ray investigations the author is indebted to professor Kato and his laboratory members. The author's thanks are especially due to Dr. Professor W. Komatsu and Dr. Y. Moriyoshi, who have given extremely valuable aid and fruitful diecussions during the work.

Nomenclature

F; flow rate of hydrogen [cc/min]
P; partial pressure of oxxgen [mmHg]
r; rate of loss-in-weight [mg-O_2/min]
$t=t_{corr}+t_0$; reduction time [min]
t_{corr}; corrected reduction time [min]
t_0; induction time [min]
$t_{0.5}$; 50% reduction time [min]
$t_{0.5corr}$; corrected 50% reduction time [min]
w; oxygen weight of hematite after reduction [mg]
w_0; initial oxygen weight of hematite [mg]
x; content of additive [atomic %]
x_{Li2O}; content of Li_2O-additive [atomic %]
$\alpha=(w_0-w)/w_0$; fractional conversion [—]
δ; electrical conductivity [1/ohm cm]

References

1) R. Schenck, H. Franz and H. W. Willke, Z. anorg. Chem., **184**, 38 (1929)
2) G. C. Williams and R. A. Ragatz, Ind. Eng. Chem., **24**, 1397 (1932)
3) ibid., **28**, 130 (1936)
4) A. Mcgeorge, A. N. Hixson and K. A. Krieger, I EC Progress Design and Development, **1**, 217 (1962)
5) von Wihelm Morawietz and Heinz-Dieler Schaefer, Arch. Eisenhüttenwes., **40**, 531 (1962)
6) S. E. Khallafalla and P. L. Weston, Trans. AIME., **239**, 1494 (1967)
7) M. Tigerschiöld, J. Iron Steel Inst., **177**, 13 (1954)
8) J. O. Edström, Jernkontorete Ann., **142**. 401 (1958)
9) Wihelm vordem Esche and Otto Steinhauer, Arch. Eisenhüttenwes., **30**, 187 (1959)
10) W. Komatsu, Y. Moriyoshi and N. Seto, Yogyo-Kyokai-Shi, **77**, 347 (1969)
11) L. S. Darken and R. N. Gurry, J. Am. Chem. Soc., **67**, 1398 (1945)
12) ibid., **68**, 798 (1946)
13) J. Feinman and J. D. Drexler, A. I. CHE. Journal, **7**. 584 (1961)
14) W. M. Mckewan, Trans. AIME., **218**, 2 (1960)
15) D. S. Tannhauser, J. Phys. Chem. Solids, **23**, 25 (1962)
16) L. Vegard, Z. Phys., **5**, 17 (1952)
17) D. W. Strckler and R. Roy, J. Am. Cerm. Soc., **44**, 225 (1961)
18) A. Muan and C. L. Gee, J. Am. Cerm. Soc. **39**, 207 (1956)